



HAL
open science

Local similarity theory as the invariant solution of the governing equations

Jun-ichi Yano, Marta Waclawczyk, Grzegorz M. Florczyk

► **To cite this version:**

Jun-ichi Yano, Marta Waclawczyk, Grzegorz M. Florczyk. Local similarity theory as the invariant solution of the governing equations. 2024. hal-04552861

HAL Id: hal-04552861

<https://hal.science/hal-04552861>

Preprint submitted on 19 Apr 2024

HAL is a multi-disciplinary open access archive for the deposit and dissemination of scientific research documents, whether they are published or not. The documents may come from teaching and research institutions in France or abroad, or from public or private research centers.

L'archive ouverte pluridisciplinaire **HAL**, est destinée au dépôt et à la diffusion de documents scientifiques de niveau recherche, publiés ou non, émanant des établissements d'enseignement et de recherche français ou étrangers, des laboratoires publics ou privés.

1 **Local similarity theory as the invariant solution of**
2 **the governing equations**

3 **Marta Waclawczyk · Jun-Ichi Yano ·**
4 **Grzegorz M. Florczyk**

5
6 Received: DD Month YEAR / Accepted: DD Month YEAR

7 DOC/PBL/Monin-Obukhov/BLM/ms.tex, March 25, 2024

8 **Abstract** The present paper shows that local similarity theories, proposed for
9 the strongly-stratified boundary layers, can be derived as invariant solutions
10 defined under the Lie-group theory. A system truncated to the mean momen-
11 tum and buoyancy equations is considered for this purpose. The study further
12 suggests how similarity functions for the mean profiles are determined from
13 the vertical fluxes, with a potential dependence on a measure of the anisotropy
14 of the system. A time scale that is likely to characterize the transiency of a
15 system is also identified as a non-dimensionalization factor.

16 **Keywords** Stably-stratified turbulence · local similarity theory · invariants ·
17 Lie symmetries

18 **1 Introduction**

19 Similarity theories are a key methodology for analyzing of flows in the atmo-
20 spheric boundary layers (ABLs). They seek universal relationships between
21 different physical variables describing the phenomenon, without explicitly solv-
22 ing the governing equations (Sorbján, 2016). The similarity theories rely on

M. Waclawczyk
Institute of Geophysics, Faculty of Physics, University of Warsaw, Warsaw, Poland E-mail:
Marta.Waclawczyk@fuw.edu.pl

J.-I. Yano
CNRM, UMR3589 (CNRS), Météo France, 31057 Toulouse Cedex, France
E-mail: jiy.gfder@gmail.com

G. M. Florczyk
Institute of Geophysics, Faculty of Physics, University of Warsaw, Warsaw, Poland E-mail:
grzegorz.florczyk@fuw.edu.pl

the so-called dimensional analyses (Barenblatt, 1996), and identify the characteristic scales to non-dimensionalize the physical variables, which fit universal curves. The first and most celebrated similarity theory of ABLs was proposed by Monin and Obukhov (1954). Those authors introduced the Obukhov length scale, L , based on the surface momentum and heat fluxes to non-dimensionalize the height, z , (Obukhov, 1948).

The standard Monin-Obukhov similarity theory (MOST) is believed to work well in the case that is homogeneous in time and space, with relatively weak stratifications. The assumed forms of the similarity functions suggest that the gradient Richardson number should tend to a constant, critical value, $Ri_{cr} \approx 0.2$, in the limit of the strong stratification. However, as the stratification further increases, turbulence tends to locally collapse, and as a result, intermittent transitions between turbulent and non-turbulent states are observed (Allouche et al., 2022; Ansorge and Mellado, 2014). This modifies the scaling of mean wind and temperature, and the Richardson number no longer levels off at Ri_{cr} .

Due to deviations of the experimental results from the MOST predictions, different theories were developed: Zilitinkevich and Calanca (2000), Zilitinkevich and Esau (2005), and Zilitinkevich and Esau (2007) introduced additional scales characterizing effect of the Earth’s rotation and the stability of free-flow. Grachev et al. (2015) considered Dougherty–Ozmidov scale, which is constructed from the turbulence kinetic energy dissipation rate. Generalization of MOST accounting for the turbulence anisotropy in ABL was proposed recently by Stiperski and Calaf (2023).

Of particular relevance for this work is the formulation of the ‘local similarity theory’ by Nieuwstadt (1984): instead of the surface values of fluxes, this theory uses their local values (i.e. measured at height z) to estimate the length scale, $\Lambda(z)$, with $\Lambda(z) \approx L$ when it is close enough to the surface. This approach was further advanced by Sorbjan (1989), who assumed more general relationships for the variation of fluxes with height.

As alternatives to the local MOST, Sorbjan (2006, 2016) proposed gradient-based similarity theories, which express the fluxes and other statistical quantities as functions of the Richardson number, Ri . These alternative formulations have advantages, over the flux-based MOST approach, of describing the weak turbulence regimes better without invoking a critical Richardson number.

This work derives the local similarity theories of a form closely following those by Sorbjan (2006, 2016), directly from the system of governing equations, instead of dimensional analyses. A similar problem was addressed by Yano and Waclawczyk (2022) with the use of the technique of non-dimensionalization (*cf.*, Yano and Bonazzola, 2009). Here, we alternatively adopt a concept of symmetries, defined by the transformations of variables that do not change the form of governing equations. The symmetries lead to invariant solutions of the considered system. By analyzing a system of governing equations as a starting point, functional relations between different variables can be derived methodologically.

68 The symmetry analysis can also reveal relations between the variables, that
 69 were previously unknown. For example, general formulas are derived for mean
 70 profiles as functions of flux-related variables. In this manner, the symmetry
 71 method can provide broader perspectives on similarity theories, by identifying
 72 assumptions behind them in a systematic way.

73 The notion of ‘invariance’ was already remarked by Monin and Obukhov
 74 (1954), although the symmetry transformations were not explicitly invoked
 75 therein. Symmetry-based methods were previously used in numerous works to
 76 obtain solutions for neutrally stratified flows in different flow configurations,
 77 e.g., Oberlack (2001), Oberlack et al. (2022), Avsarkisov et al. (2014), Sadeghi
 78 et al. (2021). Among others, the logarithmic law of the wall was derived in
 79 Oberlack and Rosteck (2010). Ji and She (2021) used symmetry-based gen-
 80 eralised dilation approach to derive expression for the mixing length in the
 81 atmospheric surface layer. The Lie symmetries for the surface layer with non-
 82 zero buoyancy were considered by Yano and Waławczyk (2023), in which
 83 the logarithmic and linear profiles for the mean wind and temperature were
 84 discussed.

85 In this paper, the local similarity theories are derived as functions of Lie
 86 group invariants of ABL flows. The local Obukhov length naturally appears
 87 in these solutions, as a combination of invariants, rather than as an externally
 88 introduced length scale. Moreover, the obtained general solutions contain de-
 89 pendencies on time, or alternatively, on a measure of anisotropy of the flow.
 90 Significantly, the derived solutions generalize the gradient-based similarity the-
 91 ories of Sorbjan (2016): the former reduces to the latter, when the Richardson
 92 number remains constant with height.

93 We consider the two distinct regions of the ABL: the outer layer, where
 94 fluxes depend on the boundary layer height, h , and the surface layer, where
 95 no external length scale governs the turbulent transports. We especially take
 96 into account an intermittency parameter, which indicates a degree that a given
 97 flow can be presented as a sum of two different contributions, e.g., turbulent
 98 and laminar, but also e.g., logarithmic and linear. When this parameter is set
 99 to zero, a solution reduces to the linear forms for mean wind and buoyancy.
 100 On the other hand, when it is non-zero, it accounts for the variability of the
 101 Richardson number at strong stratifications.

102 Seeking the universal forms of non-dimensionalized gradients of the mean
 103 wind, ϕ_m , and mean buoyancy, ϕ_h , which are independent of the local values
 104 of the intermittency parameter, we arrive, under certain assumptions, at the
 105 relations $\phi_m \sim \xi/RiG$ and $\phi_h \sim \xi/RiG^2$, where $\xi = z/L$ and the Prandtl
 106 number, G , is a function of the aspect ratio of the Reynolds stresses, which
 107 we further interpret as a measure of anisotropy of the flow. On the other
 108 hand, the analysis of experimental data from the Surface Heat Budget of
 109 the Arctic Ocean (SHEBA) experiment (Persson et al., 2002) suggests more
 110 general forms, $\phi_m \sim (\xi/RiG)^p$ and $\phi_h \sim (\xi/RiG^2)^q$ with $p = 1/3$ and $q =$
 111 -1 for very weak stratifications, and $p = 1$, $q = 1$ for strong stratifications.
 112 Furthermore, we estimate value of the intermittency parameter based on the
 113 SHEBA data.

114 The paper is organized as follows: Section 2 describes the local similarity
 115 theories in details. The symmetry methods are introduced in Sections 3 and 4.
 116 Invariants of ABL flows are discussed in Section 5. Sections 6 and 7 are devoted
 117 to the derivation of the invariant solutions in the outer and surface layer,
 118 respectively. Data analyses are performed in Section 8, followed by conclusions
 119 and perspectives.

120 2 Overview of the Local Similarity Theories

121 Processes in the atmospheric boundary layer are governed by a closed set of
 122 partial differential equations. However, due to the complexity of the processes,
 123 these equations cannot yet be solved numerically for real-world configurations.
 124 Alternatives are the similarity theories, which propose certain rescaling of the
 125 variables, that collapse the measurements collected during various experiments
 126 onto single universal curves.

127 The MOST expresses the turbulence moments as functions of the stability
 128 parameter, $\xi = z/L$, where

$$L = -\frac{1}{\kappa} \frac{|\overline{uw_0}|^{3/2}}{\overline{wb_0}} = \frac{1}{\kappa} \frac{u_*^2}{b_*} \quad (1)$$

129 is the Obukhov length, and $\overline{uw_0}$ and $\overline{wb_0}$ are the surface values of momentum
 130 and buoyancy fluxes, respectively. The buoyancy, b , is defined as

$$b = g(\theta - \theta_0(z))/\theta_m, \quad (2)$$

131 where $\theta - \theta_0(z)$ denotes deviation of the potential temperature, θ , from a steady
 132 reference state and θ_m is a vertical average. In MOST, the scales, L , $u_* =$
 133 $|\overline{uw_0}|^{1/2}$, and $u_* b_* = -\overline{wb_0}$, represent the external conditions. The similarity
 134 functions, on the other hand, express universal dependencies of turbulence
 135 moments on stability parameter ξ . In particular, Monin and Obukhov (1954)
 136 proposed to express the non-dimensional mean wind and buoyancy gradients
 137 in the stable BL as (*cf.*, Foken, 2006)

$$\frac{\kappa z}{u_*} S = \phi_m(\xi) = 1 + 5\xi, \quad (3a)$$

$$\frac{\kappa z}{b_*} N^2 = \phi_h(\xi) = 1 + 5\xi, \quad (3b)$$

138 where $S = d\bar{u}/dz$ is the mean wind shear, and $N^2 = d\bar{b}/dz$ is the square
 139 of the Brunt-Väisälä frequency. Businger et al. (1971) further elaborated the
 140 formulas, and proposed $\phi_m = 1 + 4.7\xi$ and $\phi_h = 0.74 + 4.7\xi$.

141 The question of whether the MOST correctly describes turbulence statistics
 142 in stable boundary layers (SBL), especially under weak turbulence, is subject
 143 of ongoing debate. For weak stratifications, the MOST is believed to work well
 144 within the surface layer, over which the fluxes are approximately constant with

145 height. Nieuwstadt (1984) reformulated MOST by introducing the local length
146 scale

$$\Lambda = -\frac{1}{\kappa} \frac{|\overline{w\overline{w}}|^{3/2}}{\overline{wb}} \quad (4)$$

147 as a similarity scale. In this reformulation, the equations describing relation-
148 ships between dimensionless combinations of variables were measured at the
149 same height.

150 In the outer layer, Nieuwstadt (1984) presented the momentum and buoy-
151 ancancy fluxes as functions of z/h , where h was the boundary layer height, and
152 more specifically, suggested the relations $\overline{w\overline{w}} = u_*^2(1 - z/h)^{3/2}$ and $\overline{wb} =$
153 $u_* b_* (1 - z/h)$ based on observations. Sorbjan (1989) proposed further gener-
154 alizations of the Nieuwstadt's approach by assuming the following profiles of
155 turbulent fluxes

$$\overline{w\overline{w}} = \overline{w\overline{w}}_0 \left(1 - \frac{z}{h}\right)^p, \quad \overline{wb} = \overline{wb}_0 \left(1 - \frac{z}{h}\right)^q, \quad (5)$$

156 where $p \geq q$.

157 The local scaling is valid only for strong, continuous turbulence, for the
158 subcritical values of the flux Richardson number, Ri , and, additionally, un-
159 der the assumption that Ri is constant with height (Sorbjan, 2006). These
160 conditions are not fulfilled in very stable ABLs, which consist of layered struc-
161 tures, representing a 'sporadic' turbulence intermittency. To overcome deficien-
162 cies of local similarity theory, Sorbjan (2006, 2016) proposed the alternative,
163 gradient-based scalings

$$u_N = L_N N, \quad b_N = L_N N^2, \quad L_N = l, \quad (6)$$

164 where l is a length scale, which can be defined either as the mixing length
165 $l = \kappa z$ (explicit scaling) or as a function of turbulence moments (implicit
166 scaling); u_N and b_N are the velocity and buoyancy scales constructed by using
167 L_N and the Brunt–Väisälä frequency N . For the implicit scaling, the following
168 combination can be considered (Sorbjan, 2016):

$$l = \frac{(\overline{w^2})^{1/2}}{N}. \quad (7)$$

169 In the gradient-based formulations, the Richardson number, Ri , or the flux-
170 based Richardson number, R_f , (rather than z/Λ) plays a role of stability
171 parameter. These parameters are defined by

$$Ri = \frac{N^2}{S^2}, \quad R_f = \frac{\overline{wb}}{\overline{w\overline{w}} S}. \quad (8)$$

172 It immediately follows from Eqs. (3a), (3b), and (4) that

$$Ri = \frac{z}{\Lambda} \frac{\phi_h}{\phi_m^2}. \quad (9)$$

173 Thus, Ri becomes a function of z/Λ , and as a result, Ri can be used as a
 174 vertical coordinate of the system in place of z/Λ .

175 Based on this observation, Sorbjan (2012) formulated a generalized form
 176 of the similarity theory assuming

$$\frac{l}{u_*} S = \psi_m(Ri), \quad \frac{l}{b_*} N^2 = \psi_h(Ri). \quad (10)$$

177 With $l = \kappa z$ and expressing Ri explicitly as a function of z/Λ by Eq. (9), the
 178 local MOST formulation is recovered. Moreover, Sorbjan (2016) postulated
 179 that non-dimensionalized fluxes can be presented as functions of Ri :

$$\frac{\overline{uw}}{u_N^2} = \mathcal{G}(Ri), \quad \frac{\overline{wb}}{u_N b_N} = \mathcal{H}(Ri). \quad (11)$$

180 Alternatively, non-dimensionalized turbulent fluxes as functions of R_f were
 181 considered by Łobocki (2013), Łobocki and Porretta-Tomaszewska (2021).
 182 Those authors determined the forms of \mathcal{G} and \mathcal{H} based on the Mellor–Yamada
 183 turbulence–closure model. Advantage of the gradient-based scaling is that u_N
 184 is less sensitive to sampling errors and the choice of averaging window than
 185 u_* . Moreover, spurious self-correlations are avoided, when fluxes are presented
 186 as functions of Ri .

187 3 Symmetry analysis

188 3.1 Introduction

189 To derive local similarity theories from a system of governing equations, we first
 190 need to identify the transformations of the variables that leave the equations
 191 unchanged, i.e. transformations that do not affect the physics of a given system.
 192 These transformations are called the symmetries of the governing equations;
 193 the concept was first introduced by a Norwegian mathematician Sophus Lie in
 194 the second half of the 19th century. In the following, we apply symmetry anal-
 195 yses for deriving these transformations to the two examples: Monin–Obukhov
 196 arguments on invariant functions and by analyzing symmetries of the diffusion
 197 equation.

198 3.2 Monin–Obukhov

Even though the Lie symmetries were not explicitly mentioned by Monin and
 Obukhov (1954), those authors used a similar concept, namely the concept of
 invariant. Let the variables z and t transform into a new set of independent
 variables z^* and t^* . Also, a dependent variable, say $\theta(z, t)$, is transformed to
 $\theta^*(z^*, t^*)$. An invariant is a function $C(\theta, z, t)$, which preserves its form when
 it is written in terms of the new variables:

$$C(\theta, z, t) = C(\theta^*, z^*, t^*).$$

199 Monin and Obukhov (1954) argued that statistical characteristics of the rela-
 200 tive movements in a stream are invariant with respect to the following simi-
 201 larity transformations

$$x^* = \lambda x, \quad y^* = \lambda y, \quad z^* = \lambda z, \quad t^* = \lambda t. \quad (12)$$

It was also implicitly assumed that the system is conserved by the translation of the mean wind velocity:

$$\bar{u}^* = \bar{u} + \bar{u}_0.$$

Consequently, Monin and Obukhov (1954) considered difference of velocities at two different heights. In this case the translation shifts cancel, and

$$\bar{u}^*(z_2^*) - \bar{u}^*(z_1^*) = \bar{u}(z_2) - \bar{u}(z_1)$$

202 is an invariant with respect to all the above transformations. As argued by
 203 those authors, the non-dimensional magnitude is a function of both z_1 and
 204 z_2 , but because it must also be invariant under the scaling (12), it must be a
 205 function of the ratio z_2/z_1

$$\frac{\bar{u}(z_2) - \bar{u}(z_1)}{u_*} = f\left(\frac{z_2}{z_1}\right). \quad (13)$$

206 Monin and Obukhov (1954) used the form (13) to derive the logarithmic so-
 207 lution for the mean wind.

208 3.3 Diffusion Equation

209 We briefly present the main concepts of the Lie group analysis, taking as an
 210 example, the one-dimensional heat equation

$$\frac{\partial \theta}{\partial t} = \frac{\partial^2 \theta}{\partial z^2} \quad (14)$$

211 with the initial condition $\theta(z, 0) = \delta(z)$.

212 It can easily be verified that this equation remains unchanged under the
 213 transformations of θ , z and t into:

$$z^* = \lambda z, \quad t^* = \lambda^2 t, \quad \theta^* = \theta/\lambda, \quad (15)$$

214 where $\lambda > 0$ is a constant, *i.e.*, (15) are symmetry transformations, which
 215 represent symmetries of the problem (14). It can be shown that they form a
 216 mathematical object called a group.

217 3.4 Group and Invariant Transformations

218 Mathematically, a group consists of a non-empty set and a pre-defined operation
 219 tion, in which a third element, that is created by combining any two arbitrary
 220 elements by the given operation, must also be an element of this set. Addi-
 221 tionally required conditions are: the operation must be associative; an identity
 222 element must exist; and every element must have an inverse.

All the properties of the group are satisfied by the transformation (15). It can be demonstrated by presenting (15) in the exponential form $z^* = \lambda z = e^\epsilon z$, where $\epsilon \in \mathbb{R}$. Combination of two transformations

$$z^* = e^{\epsilon_1} (e^{\epsilon_2} z)$$

is a new transformation

$$z^* = e^{\epsilon_1 + \epsilon_2} z = e^\epsilon z.$$

The unitary element of the transformation is obtained by setting $\epsilon = 0$. The inverse element is derived by replacing ϵ by $-\epsilon$, so that

$$z^* = e^\epsilon e^{-\epsilon} z = z.$$

223 The associativity property is also satisfied by $z^* = (e^{\epsilon_1} e^{\epsilon_2}) e^{\epsilon_3} z = e^{\epsilon_1} (e^{\epsilon_2} e^{\epsilon_3}) z$.

224 The Lie group analysis is a method of determining Lie symmetry trans-
 225 formations of a given differential equation system. This, in turn, allows us to
 226 derive invariants and invariant solutions. Details of the Lie group analysis are
 227 beyond the scope of this paper, and an interested reader is referred to text-
 228 books, e.g. Bluman and Kumei (1989). Also computer algebra systems can be
 229 used to identify all symmetries of a given, closed system of equations. The
 230 next important step is a derivation of invariant solutions from a given set of
 231 symmetry transformations. This study focuses on this second step.

232 For this purpose, we introduce infinitesimal forms by expanding the global
 233 transformation forms, z^* , t^* and θ^* , in the Taylor series around $\epsilon = 0$:

$$\begin{aligned} z^* &= z + \left. \frac{dz^*}{d\epsilon} \right|_{\epsilon=0} \epsilon + \mathcal{O}(\epsilon^2), & t^* &= t + \left. \frac{dt^*}{d\epsilon} \right|_{\epsilon=0} \epsilon + \mathcal{O}(\epsilon^2), \\ \theta^* &= \theta + \left. \frac{d\theta^*}{d\epsilon} \right|_{\epsilon=0} \epsilon + \mathcal{O}(\epsilon^2); \end{aligned} \quad (16)$$

The first-order derivatives at $\epsilon = 0$ are called “infinitesimals”, and will be denoted by ξ_z , ξ_t and η . As the Lie’s theorem states, the global forms of transformations, z^* , t^* and θ^* , are obtained by integrating the infinitesimal forms:

$$\frac{dz^*}{d\epsilon} = \xi_z(z^*, t^*, \theta^*), \quad \frac{dt^*}{d\epsilon} = \xi_t(z^*, t^*, \theta^*), \quad \frac{d\theta^*}{d\epsilon} = \eta(z^*, t^*, \theta^*)$$

234 with the initial conditions $z^* = z$, $t^* = t$, and $\theta^* = \theta$ at $\epsilon = 0$. In this manner,
 235 the infinitesimal and global forms become equivalent.

236 The infinitesimal generator, X , of the transformations for the heat equation
 237 is defined by

$$X = \xi_z(z, t, \theta) \frac{\partial}{\partial z} + \xi_t(z, t, \theta) \frac{\partial}{\partial t} + \eta(z, t, \theta) \frac{\partial}{\partial \theta}. \quad (17)$$

238 The solution $\theta = \Theta(z, t)$ is an invariant solution of the heat equation (14), if
 239 and only if it satisfies equation

$$X(\theta - \Theta(z, t)) = \xi_z(z, t, \theta) \frac{\partial \Theta}{\partial z} + \xi_t(z, t, \theta) \frac{\partial \Theta}{\partial t} + \eta(z, t, \theta) = 0, \quad (18)$$

240 and solves Eq. (14).

241 The condition (18) can be solved by a method of characteristics, solving
 242 the corresponding characteristic equation:

$$\frac{dz}{\xi_z(z, t, \theta)} = \frac{dt}{\xi_t(z, t, \theta)} = \frac{d\theta}{\eta(z, t, \theta)}. \quad (19)$$

243 As an example, let us consider the scaling transformations (15), and rewrite
 244 them as $z^* = e^\epsilon z$, $t^* = e^{2\epsilon} t$, $\theta^* = e^{-\epsilon} \theta$. Infinitesimal forms of these transfor-
 245 mations are, as defined by Eq. (16),

$$z^* = z + \xi_z \epsilon + \mathcal{O}(\epsilon^2) = z + z\epsilon + \mathcal{O}(\epsilon^2), \quad (20a)$$

$$t^* = t + \xi_t \epsilon + \mathcal{O}(\epsilon^2) = t + 2t\epsilon + \mathcal{O}(\epsilon^2), \quad (20b)$$

$$\theta^* = \theta + \eta \epsilon + \mathcal{O}(\epsilon^2) = \theta - \theta\epsilon + \mathcal{O}(\epsilon^2), \quad (20c)$$

246 and the corresponding characteristic equation (19) reads

$$\frac{dz}{z} = \frac{dt}{2t} = \frac{d\theta}{-\theta}. \quad (21)$$

247 3.5 Invariant Solutions

248 Solving for the two equalities in Eq. (21), we find two invariants X and C

$$X = \frac{z}{\sqrt{t}}, \quad C = \sqrt{t} \theta, \quad (22)$$

249 which remain unchanged when written in new variables (15). The relations
 250 (22) correspond e.g. to characteristic curves obtained by Riehm's method
 251 in wave dynamics (Lighthill, 1978). The solution of Eq. (21) is given implicitly
 252 by the invariant form

$$C = F(X), \quad \text{hence} \quad \theta = \frac{1}{\sqrt{t}} F\left(\frac{z}{\sqrt{t}}\right), \quad (23)$$

253 where F is an arbitrary function. Here, an invariant, X , from now on, plays a
 254 role of an independent variable of the system.

255 Substituting (23) into the heat equation (14), we obtain a reduced equation
 256 with one independent variable X ,

$$2F'' + C_1F' + F = 0, \quad (24)$$

257 which determines the form of the function F .

258 Note that invariance under the scaling groups is linked to the dimensional
 259 analysis and the Buckingham Pi–theorem (Buckingham, 1914). As argued by
 260 Bluman and Kumei (1989), if a dimensional analysis leads to a reduction of
 261 the number of independent variables, then such a reduction is always possible
 262 through invariance under scalings; however, the opposite is not always true.
 263 In this manner, the invariance of variables under scaling groups is considered
 264 a generalization of the dimensional analyses.

265 The main goal of this work is to present a solution of a boundary–
 266 layer system as a function of invariant variables. Here, considered dependent
 267 variables are: the mean velocity and buoyancy gradients, S , N^2 , as well as the
 268 mean pressure \bar{p} , fluxes \overline{uw} , \overline{wb} and the variance $\overline{w^2}$. As a consequence, the
 269 local similarity theory is directly derived from the set of governing equations
 270 in an invariant form as given by Eq. (23).

271 4 Lie group analysis of the governing equations

272 4.1 Governing equations

273 We consider flows in the atmospheric boundary layer, governed by the Navier–
 274 Stokes system under the Boussinesq approximation and in the inviscid limit.
 275 We perform ensemble averaging of the prognostic equations, and as a result,
 276 any physical variable, ϕ , is decomposed into mean and fluctuation, *i.e.*, $\phi = \bar{\phi} +$
 277 ϕ' , as usually considered in turbulence studies. However, by following Oberlack
 278 et al. (2022), we consider ensemble averages of total quantities, *e.g.* \overline{uw} rather
 279 than of fluctuations, $\overline{u'w'}$, because the equation system becomes linear in terms
 280 of those total averages. In some cases, the averages of instantaneous variables
 281 will be identical to the correlations of fluctuations, *e.g.* if $\bar{w} = 0$, we have $\overline{uw} =$
 282 $\overline{u'w'}$ and $\overline{wb} = \overline{w'b'}$. However, the same does not automatically apply to the
 283 other statistics. Furthermore, we assume that horizontal gradients of velocity
 284 moments are smaller than the vertical gradient by an order of magnitude, and
 285 that the Coriolis force is balanced by the horizontal pressure gradients, thus by
 286 subtracting the geostrophic–pressure component, the Coriolis force no longer
 287 plays an explicit role. In the following, the horizontal coordinate, x , is taken
 288 as the direction of the mean wind.

289 Under those assumptions, the governing equation system reads

$$\frac{\partial \bar{u}}{\partial t} + \frac{\partial \bar{u}\bar{w}}{\partial z} = 0, \quad (25a)$$

$$\frac{\partial \bar{w}^2}{\partial z} = -\frac{1}{\rho_0} \frac{\partial \bar{p}}{\partial z} + \bar{b}, \quad (25b)$$

$$\frac{\partial \bar{b}}{\partial t} + \frac{\partial \bar{w}\bar{b}}{\partial z} = 0, \quad (25c)$$

290 where ρ_0 is a constant mean density, and p is the pressure.

291 The system (25a)–(25c) is unclosed, because there are more dependent vari-
 292 ables than an available number of equations. It is well known in the boundary-
 293 layer meteorology that for solving this differential equation system, a certain
 294 closure is required. Yet, it is still possible to consistently identify the transfor-
 295 mation rules to all the dependent variables as well as coordinates (independent
 296 variables) of the system that conserves the given equation set (Oberlack and
 297 Rosteck, 2010). From those identified transformation rules, it is also possible
 298 to derive the invariant solutions of the system. Importantly, those obtained
 299 invariant solutions still constitute special solutions of a given system, even
 300 though the system is underdetermined.¹

301 4.2 Groups of transformations: List

302 The purpose of this subsection is to present the symmetry transformations sat-
 303 isfied by this system one by one with the considerations of their characteristics.
 304 We consider the symmetries of the Navier-Stokes equations with zero viscosi-
 305 ty (*cf.*, Pukhnachev, 1972), and, additionally, the invariance under scaling
 306 and groups of translations of an infinite hierarchy of equations for moments
 307 (Oberlack and Rosteck, 2010).

308 Eqs. (25a)–(25c) are invariant under the time and space translations:

$$t^* = t + t_0, \quad (26a)$$

$$\mathbf{x}^* = \mathbf{x} + \mathbf{f}(t), \quad \bar{\mathbf{u}}^* = \bar{\mathbf{u}} + \frac{d\mathbf{f}(t)}{dt}, \quad \bar{p}^* = \bar{p} - \mathbf{x} \cdot \frac{d^2\mathbf{f}(t)}{dt^2}, \quad (26b)$$

309 where $\mathbf{u} = (u, v, w)$, $\mathbf{x} = (x, y, z)$, and $\mathbf{f}(t)$ is an arbitrary vector function of
 310 time. It is invariant furthermore, under a rotations on the x - y plane, under
 311 pressure translations $\bar{p}^* = \bar{p} + g(t)$ with $g(t)$ an arbitrary function of time, as
 312 well as under the translations

$$\bar{b}^* = \bar{b} + b_0, \quad \bar{p}^* = \bar{p} + z\rho_0 b_0. \quad (26c)$$

¹ Formal mathematical issues yet still remain due to the more dependent variables than available equations. These issues may be avoided by treating an excess of dependent variables as *external functions*: those external functions must also be transformed in a similar manner as proper dependent variables. To elucidate those mathematical subtleties, Frewer et al. (2015) suggest to call the invariances for these external functions to be “equivalence” rather than “symmetry” transformations.

313 The two further scaling-group symmetries are included for the considera-
314 tions:

$$t^* = t, \quad z^* = e^{a_z z}, \quad \bar{u}^* = e^{a_z \bar{u}}, \quad \bar{b}^* = e^{a_z \bar{b}}, \quad \bar{p}^* = e^{2a_z \bar{p}}, \quad (26d)$$

$$\begin{aligned} \overline{uw}^* &= e^{2a_z \overline{uw}}, & \overline{w^2}^* &= e^{2a_z \overline{w^2}}, & \overline{wb}^* &= e^{2a_z \overline{wb}}, \\ t^* &= e^{a_t t}, & z^* &= z, & \bar{u}^* &= e^{-a_t \bar{u}}, & \bar{b}^* &= e^{-2a_t \bar{b}}, & \bar{p}^* &= e^{-2a_t \bar{p}}, \\ \overline{uw}^* &= e^{-2a_t \overline{uw}}, & \overline{w^2}^* &= e^{-2a_t \overline{w^2}}, & \overline{wb}^* &= e^{-3a_t \overline{wb}}, \end{aligned} \quad (26e)$$

315 They will become particularly important for the derivation of scaling laws in
316 the following.

317 When the buoyancy \bar{b} can be neglected in the momentum equation (25b),
318 *e.g.*, under the neutral stratifications, an additional, independent scaling group
319 for the buoyancy exists:

$$\bar{b}^* = e^{a_b \bar{b}}. \quad (26f)$$

320 Refer to the discussions in the Appendix of Yano and Waclawczyk (2023) for
321 more details.

322 As shown by Oberlack and Rosteck (2010), Eqs. (25a)–(25c) are invariant
323 under additional translations due to their linearities: see also Waclawczyk et al.
324 (2017). Generally, arbitrary known solutions of a linear system can be added to
325 the variables by a linear superposition principle. However, we will only include
326 translations by a constant in the following, because this form of translation
327 for the mean velocity leads to the logarithmic solution identified by Monin
328 and Obukhov (1954):

$$\bar{u}^* = \bar{u} + u_0, \quad \bar{b}^* = \bar{b} + b_0, \quad (27a)$$

$$\overline{uw}^* = \overline{uw} + uw_0, \quad \overline{wb}^* = \overline{wb} + wb_0, \quad \overline{w^2}^* = \overline{w^2} + w_0^2 \quad (27b)$$

329 A further statistical scaling group is identified in Khujadze and Oberlack
330 (2004), Oberlack and Rosteck (2010) :

$$\begin{aligned} t^* &= t, & z^* &= z, & \bar{u}^* &= e^{a_s \bar{u}}, & \bar{b}^* &= e^{a_s \bar{b}}, & \bar{p}^* &= e^{a_s \bar{p}}, \\ \overline{uw}^* &= e^{a_s \overline{uw}}, & \overline{w^2}^* &= e^{a_s \overline{w^2}}, & \overline{wb}^* &= e^{a_s \overline{wb}}. \end{aligned} \quad (27c)$$

331 The invariance of the system (25a)–(25c) under the above transformations can
332 be verified in a straightforward manner by direct substitutions. Transformations
333 (27b) and (27c) have no correspondence in symmetries of the instantaneous
334 velocity u and buoyancy b . For this reason, they are referred “statistical
335 groups”. The statistical scaling basically represents the fact that if the set of
336 variables \bar{u} , \overline{uw} , \overline{wb} , $\overline{w^2}$, \bar{p} , \bar{b} solves equations (25a)–(25c), then, due to their
337 linearity, also does the set $\gamma \bar{u}$, $\gamma \overline{uw}$, $\gamma \overline{wb}$, $\gamma \overline{w^2}$, $\gamma \bar{p}$, $\gamma \bar{b}$ where

$$\gamma = e^{a_s}. \quad (28)$$

338 Waclawczyk et al. (2014) related the statistical scaling to the phenomenon
339 of intermittency, understood as alternating occurrence of laminar and turbulent
340 flows. If we consider two different types of solutions of the equations (*e.g.*

341 turbulent and laminar), denoting them by indices 1 and 2, a solution can be
 342 presented by a weighted sum of conditional statistics:

$$\bar{u}^* = \gamma \bar{u}_1 + (1 - \gamma) \bar{u}_2, \quad \bar{b}^* = \gamma \bar{b}_1 + (1 - \gamma) \bar{b}_2, \quad (29)$$

343 where $0 \leq \gamma \leq 1$ becomes an intermittency factor, if $a_s \leq 0$. γ is equal to
 344 the unity when the flow is fully turbulent, and vanishes when it is purely
 345 laminar. Because a_s is restricted to $a_s < 0$, the transformations (27c) form a
 346 semi-group.

347 Such a representation is linked to observations in very stable atmospheric
 348 boundary layers. As discussed by Allouche et al. (2022), the analysis in the
 349 intermittent regime cannot rely on bulk statistics, but may require conditional
 350 analysis. More generally, conditional statistics with indices 1 and 2 could refer
 351 to some limit cases, *e.g.*, a logarithmic function in neutral limit and a linear in
 352 the strongly stratified limit. The final solution can be represented as a weighted
 353 sum of these two limiting solutions.

354 Finally, when the Coriolis force is taken into account, the rotation, time
 355 scaling, and the statistical scaling group are modified to a more complex form,
 356 (*cf.*, Rosteck, 2014). It is left for a future study to consider these modifica-
 357 tions. Here, we assume that the statistics are not influenced by the Earth's
 358 rotation, although for large stratifications this assumption may be too strong.
 359 In this work, horizontal transports are also neglected. This simplification does
 360 not affect the scaling symmetries (26d)–(26e), which are the same as in the
 361 underlying Navier-Stokes system. Furthermore, the invariance due to the sta-
 362 tistical scaling group (27c) is a property of equations for moments in their
 363 general form, *i.e.* with the horizontal transport terms (*cf.*, Oberlack and Ros-
 364 teck, 2010).

365 5 Invariants of boundary–layer flows

366 5.1 Characteristic system

367 In deriving the invariants of the boundary–layer flows, we take into account
 368 the time translation symmetry (26a) and the space translation (26b), assuming
 369 that $\mathbf{f}(t) = \mathbf{x}_0$ is a constant vector, the scaling groups (26d)–(26e), as well as
 370 the statistical scaling and translations (27b), (27c). Consequently, we obtain

371 the following characteristic system:

$$\begin{aligned}
\frac{dt}{a_t(t-t_0)} &= \frac{dz}{a_z(z-z_0)} = \frac{d\bar{w}\bar{b}}{(2a_z-3a_t+a_s)(\bar{w}\bar{b}-wb_0)} = \\
&= \frac{d\bar{u}\bar{w}}{(2a_z-2a_t+a_s)(\bar{u}\bar{w}-uw_0)} = \frac{dw^2}{(2a_z-2a_t+a_s)(\bar{w}^2-w_0^2)} = \\
&= \frac{d\bar{b}}{(a_z-2a_t+a_s)(\bar{b}-b_0)} = \frac{d\bar{u}}{(a_z-a_t+a_s)(\bar{u}-u_0)} = \\
&= \frac{d\bar{p}}{(2a_z-2a_t+a_s)(\bar{p}-p_0-zb_0\rho_0\alpha)}, \quad (30)
\end{aligned}$$

372 where $\alpha = (a_z - 2a_t + a_s)/(2a_z - 2a_t + a_s)$. Solving the system (30), we obtain
373 the 7 invariants:

$$t - t_0 = X_t |z - z_0|^\beta \quad (31a)$$

$$\bar{u} - u_0 = C_u |z - z_0|^{1-\beta+\chi}, \quad (31b)$$

$$\bar{b} - b_0 = C_b |z - z_0|^{1-2\beta+\chi}, \quad (31c)$$

$$\frac{\bar{p}}{\rho_0} - \frac{p_0}{\rho_0} = C_p |z - z_0|^{2-2\beta+\chi} - \frac{b_0\alpha[z_0 - (2-2\beta+\chi)z]}{1-2\beta+\chi}, \quad (31d)$$

$$\bar{u}\bar{w} - uw_0 = C_1 |z - z_0|^{2-2\beta+\chi}, \quad (31e)$$

$$\bar{w}^2 - w_0^2 = C_2 |z - z_0|^{2-2\beta+\chi}, \quad (31f)$$

$$\bar{w}\bar{b} - wb_0 = C_3 |z - z_0|^{2-3\beta+\chi}, \quad (31g)$$

374 where

$$\beta = a_t/a_z, \quad \text{and} \quad \chi = a_s/a_z. \quad (31h)$$

375 5.2 Invariant solutions

376 The invariants, C_u , C_p , C_b , C_1 , C_2 and C_3 are functions of the new variable
377 X_t , introduced by Eq. (31a), so that the invariant solutions (23) are generated
378 as:

$$C_u = F(X_t), \quad C_p = G(X_t), \quad C_b = H(X_t), \quad (32a)$$

$$C_1 = C_1(X_t), \quad C_2 = C_2(X_t), \quad C_3 = C_3(X_t). \quad (32b)$$

379 After introducing these invariants into the system (25a–(25c), the relations
380 between C_u , C_b , C_p and remaining invariants can be derived.

381 In the following, we analyze the invariant solutions in the outer and surface
382 layers of ABL separately: we expect that the statistics in the outer layer are
383 influenced by the boundary layer height, h , but not the statistics of the surface
384 layer.

385 6 Local similarity — outer layer

386 6.1 Invariants

387 The constant z_0 in Eqs. (31a)–(31g) can be chosen in various ways, depending
 388 on the flow configuration. For the outer layer, we assume that $z_0 = h$, and that
 389 $u_0 = \bar{u}(h)$ and $b_0 = \bar{b}(h)$ play the roles of the velocity and buoyancy scales.
 390 With this choice, the heat and momentum fluxes change with the height as
 391 proposed by Sorbjan (1989), cf., his Eqs. (5). These forms are obtained as
 392 invariants by setting $z_0 = h$ in Eqs. (31a) – (31g). Then, the fluxes read

$$\overline{uw} = C_1(X_t) \left(1 - \frac{z}{h}\right)^{2-2\beta+\chi}, \quad (33a)$$

$$\overline{w^2} = C_2(X_t) \left(1 - \frac{z}{h}\right)^{2-2\beta+\chi}, \quad (33b)$$

$$\overline{wb} = C_3(X_t) \left(1 - \frac{z}{h}\right)^{2-3\beta+\chi}. \quad (33c)$$

393 Those invariants can be rearranged to more convenient forms:

$$S = \frac{d\bar{u}}{dz} = \tilde{C}_u(X_t) \left(1 - \frac{z}{h}\right)^{\chi-\beta}, \quad (34a)$$

$$N^2 = \frac{d\bar{b}}{dz} = \tilde{C}_b(X_t) \left(1 - \frac{z}{h}\right)^{\chi-2\beta}, \quad (34b)$$

$$\frac{\overline{uw}}{\overline{w^2}} = \frac{C_1(X_t)}{C_2(X_t)} = f(X_t), \quad (34c)$$

$$\frac{\overline{wb}}{\overline{uw}} \left(1 - \frac{z}{h}\right)^\beta = \frac{C_3(X_t)}{C_1(X_t)} = g(X_t), \quad (34d)$$

$$\frac{\overline{wb}}{\overline{uw}} (t - t_0) = \frac{C_3(X_t)X_t}{C_1(X_t)} = q(X_t). \quad (34e)$$

394 Here, we have skipped the expression for the pressure, which is usually not
 395 considered as a part of similarity theories. Eqs. (34a) and (34b) together with
 396 formulas (34c)–(34e) lead to local similarity formulas as going to be shown
 397 below. The ratios of fluxes in Eqs. (34c) – (34e) become functions of X_t .
 398 Moreover, the ratio C_3/C_1 from Eq. (34d) can be rearranged as follows

$$\frac{C_3(X_t)}{C_1(X_t)} = -\sqrt{|\overline{uw}|} \frac{\overline{wb}}{|\overline{uw}|^{3/2}} \left(1 - \frac{z}{h}\right)^\beta = \frac{\sqrt{|\overline{uw}|}}{\kappa\Lambda} \left(1 - \frac{z}{h}\right)^\beta. \quad (35)$$

399 Remarkably, in Eq. (35), we find the local Obukhov length, Λ , defined in
 400 Eq. (4), which is one of the possible local length scales suggested in the local
 401 similarity theories (Nieuwstadt, 1984). The ratio between the buoyancy and
 402 momentum fluxes is also found in Eq. (34e) as a factor to non-dimensionalize
 403 the time. All invariants can additionally depend on the characteristic scales of
 404 the system: h , u_0 and b_0 when needed for dimensional consistency.

6.2 Similarity solutions

To derive formulas for S and N^2 in terms of fluxes, we substitute the factor $(1 - z/h)^\beta$ calculated from Eq. (35) into Eqs. (34a) and (34b). We also assume that relations (34c) and (34e) can be inverted over a time interval, $\Delta t = t - t_0$, so that

$$\frac{u_0}{h} X_t = f^{-1} \left(\frac{\overline{uw}}{w^2} \right), \quad \frac{u_0}{h} X_t = q^{-1} \left(\frac{\overline{wb}}{\overline{uw}} (t - t_0) \right), \quad (36)$$

where the factor u_0/h has been included for the dimensional consistency. We take into account the first from relations (36). With this we obtain

$$S = \frac{\sqrt{|\overline{uw}|}}{\kappa A} \left(1 - \frac{z}{h} \right)^x F \left(\frac{|\overline{uw}|}{w^2} \right), \quad (37a)$$

$$N^2 = - \frac{\overline{wb}}{\sqrt{|\overline{uw}|}} \frac{1}{\kappa A} \left(1 - \frac{z}{h} \right)^x H \left(\frac{|\overline{uw}|}{w^2} \right). \quad (37b)$$

In addition to the local Obukhov length A , S and N^2 also depend on a height-dependent prefactor, $(1 - z/h)^x$ and the non-dimensional parameter, $|\overline{uw}|/w^2$ through the similarity functions, F and H . Alternatively, F and H can be written as functions of the non-dimensional time, $(t - t_0)\overline{wb}/\overline{uw}$. In this manner, standard similarity solutions for the shear, S , and the stratification, N , are obtained formally under a quasi-stationary state as invariant solutions. Yet, it is worthwhile to note a crucial role played by a time-dependent characteristic, X_t , in deriving these quasi-stationary solutions; it further suggests that a weak transiency of the system, represented by X_t , plays a crucial role in determining those standard quasi-stationary state of the boundary layer.

The parameter, $|\overline{uw}|/w^2$, can be interpreted as an aspect ratio of turbulent eddies in anisotropic flows. Stiperski et al. (2021) and Stiperski and Calaf (2023) suggest that departure of the scaling from the MOST is strongly correlated to the anisotropy of the Reynolds stress tensor. Some studies propose additional dependencies representing degrees of turbulence to the similarity functions under strong stratifications. For example, Klipp and Mahrt (2004) introduce a vertical-velocity variance threshold to filter out weak turbulence regimes. The analysis here points out more objectively that $|\overline{uw}|/w^2$ is an additional dependent variable that characterizes the similarity functions.

The non-dimensional time, $(t - t_0)\overline{wb}/\overline{uw}$, represents a time dependence of the similarity functions for the mean wind shear and the stratification. We expect that the transiency characterized by this non-dimensional time becomes important under strong stratifications. Importantly, the time is non-dimensionalized by the scale, $\overline{uw}/\overline{wb}$, thus a frequency distribution of $\overline{uw}/\overline{wb}$ should reveal the actual characteristic time scales of the system.

437 6.3 Richardson and Prandtl numbers

438 As an important direct consequence from Eqs. (37a) and (37b), we derive the
439 Richardson number as:

$$440 \quad Ri = \frac{N^2}{S^2} = \left(1 - \frac{z}{h}\right)^{-x} \frac{H}{F^2}. \quad (38)$$

440 By inverting the above relation, $\overline{uw}/\overline{w^2}$ is extracted into:

$$\frac{|\overline{uw}|}{\overline{w^2}} = \mathcal{G} \left[Ri \left(1 - \frac{z}{h}\right)^x \right], \quad (39)$$

441 where \mathcal{G} is a function obtained by an inversion. Furthermore, by introducing
442 the definitions of the local non-dimensional functions ϕ_h and ϕ_m into Eqs.
443 (37a) and (37b), we obtain

$$\phi_m = \frac{\kappa z}{\sqrt{|\overline{uw}|}} S = \frac{z}{\Lambda} \left(1 - \frac{z}{h}\right)^x F, \quad (40a)$$

$$\phi_h = \kappa z \frac{\sqrt{|\overline{uw}|}}{-wb} N^2 = \frac{z}{\Lambda} \left(1 - \frac{z}{h}\right)^x H. \quad (40b)$$

444 It follows from these two relations that the turbulent Prandtl number, $Pr_t =$
445 ϕ_h/ϕ_m , is not a constant, but is a function of the non-dimensional ratio
446 $|\overline{uw}|/\overline{w^2}$, or the non-dimensionalized time *i.e.*,

$$Pr_t = \frac{\phi_h}{\phi_m} = \frac{H}{F} \neq const. \quad (41)$$

447 A standard similarity theory for the surface layer predicts that the universal
448 functions, ϕ_m and ϕ_h , are linear in their argument $\xi = z/L$ for weak strati-
449 fications. If we assume the same for the local similarity, *i.e.* that ϕ_m and ϕ_h
450 are proportional to z/Λ , it then follows that the turbulent Prandtl number
451 should be constant. Here, the derived solutions (40a, b) and (41) predict the
452 deviations from those predictions in the outer layer.

453 6.4 Relations to the gradient-based similarity theory

454 Equation (39) with the dependence on Ri suggests a link to the Sorbjan's
455 gradient-based similarity theory (*cf.*, Sorbjan, 2006, 2010, 2016). We now
456 examine under what conditions the derived relationships reduce to this theory.

457 For this purpose, we adopt the scales $u_N^2 = \overline{w^2}$ and $b_N = u_N N$ defined by
458 Eqs. (6) and (7). The relation (39) defined in the previous subsection already
459 presents the momentum flux, \overline{uw} , non-dimensionalized by the scale u_N :

$$|\overline{uw}| = u_N^2 \mathcal{G} \left[Ri \left(1 - \frac{z}{h}\right)^x \right]. \quad (42)$$

460 To derive a formula for the buoyancy flux, we replace the ratio C_3/C_1 defined
461 in Eq. (34d) by the ratio C_3/C_2

$$\frac{C_3}{C_2} = \frac{\overline{wb}}{w^2} \left(1 - \frac{z}{h}\right)^\beta = \frac{\overline{wb}}{u_N^2} \left(1 - \frac{z}{h}\right)^\beta, \quad (43)$$

462 and rewrite Eq. (37b) as

$$N^2 = \frac{\overline{wb}^2}{u_N^4} \left(1 - \frac{z}{h}\right)^\chi H \left(\frac{|\overline{ww}|}{u_N^2}\right). \quad (44)$$

463 Applying the square root on (44) and after some rearrangements, we obtain

$$\overline{wb} = Nu_N^2 \left(1 - \frac{z}{h}\right)^{-\chi/2} \mathcal{H} \left[Ri \left(1 - \frac{z}{h}\right)^\chi \right], \quad (45)$$

464 where we have also replaced the first argument of the function H in Eq. (44)
465 by taking into account of Eq. (42). Finally, when $\chi = 0$, Eqs. (42) and (45)
466 become functions of Ri only, as predicted by Sorbjan (2016), cf., Eq. (11):

$$\overline{ww} = u_N \mathcal{G}(Ri), \quad \overline{wb} = N \overline{w^2} \mathcal{H}(Ri) = b_N u_N \mathcal{H}(Ri). \quad (46)$$

467 7 Local similarity — surface layer

468 The surface layer is a region adjacent to the Earth's surface, where turbu-
469 lent fluxes are believed to remain approximately constant with height. In this
470 layer, we can assume that the statistics are not influenced by the boundary
471 layer height, h , except for the case with strong stratifications. A local sim-
472 ilarity theory can be derived from the given symmetries, but by proceeding
473 differently: instead of h , the characteristic surface roughness, d , is introduced
474 as an external length.

475 By deriving a local similarity from the given symmetries, the Obukhov
476 length enters the solution as a combination of invariants, but this time only in
477 the limit of the weak stratification when the local Obukhov length is approx-
478 imately equal to its surface value.

479 7.1 Neutral stratification

480 A region adjacent to the Earth's surface is affected by the surface roughness
481 with the characteristic length, d . On the other hand, the statistics at higher
482 altitudes are affected by another length scale — the boundary layer height,
483 h . We assume that between these two regions, there exists a transition layer,
484 where turbulent transport is affected neither by d nor h . We will hence expect
485 that the gradient of velocity as well as the fluxes in the transition layer will
486 not depend on d . Under the neutral stratification this requirement leads to the
487 logarithmic solution. Logarithmic solution for near-wall flows was derived by

488 Oberlack (2001) and Oberlack and Rosteck (2010) based on the symmetries
 489 of Navier–Stokes and statistical scaling and translation groups. Here, we first
 490 address the arguments of Monin and Obukhov (1954), who stated that the
 491 statistical characteristics of the relative movements in the neutral ABL are
 492 invariant with respect to space and time scaling prescribed by Eqs. (12). Their
 493 transformations for space and time are written in the global form, with $\lambda =$
 494 $e^{a_z} = e^{a_t}$. Hence, these transformations are equivalent to setting $a_z = a_t$, thus
 495 $\beta = 1$. The invariance of the relative movements is further obtained by setting
 496 $a_s = 0$. It follows that, instead of Eq. (30), we consider the following reduced
 497 characteristic system for velocity statistics

$$\frac{dt}{a_z(t-t_0)} = \frac{dz/d}{a_z(z-z_0)/d} = \frac{d\bar{u}}{-\tilde{u}_0} = \frac{d\overline{uw}}{0} = \frac{d\overline{w^2}}{0}, \quad (47)$$

498 where we have defined $\tilde{u}_0 = \bar{u}_0/(a_z - a_t + a_s)$. As \bar{u}_0 is an arbitrary constant, we
 499 can assume that $\bar{u}_0/(a_z - a_t + a_s)$ remains finite in the limit of $a_z - a_t + a_s \rightarrow 0$.
 500 We also assume the zero translational constants, $uw_0 = 0$ and $w_0^2 = 0$, as
 501 suggested by division by zero in the last two terms. Furthermore, we have
 502 introduced d as an external length scale. Solving Eq. (47), we obtain the 4
 503 invariants, C_u , C_1 , C_2 and X_t , which express a logarithmic profile for the
 504 mean velocity:

$$\begin{aligned} \bar{u} &= \frac{-\bar{u}_0}{a_z} \ln \frac{(z-z_0)}{d} + C_u(X_t), \\ \overline{uw} &= C_1(X_t), \quad \overline{w^2} = C_2(X_t), \quad X_t = \frac{(t-t_0)d}{z-z_0}. \end{aligned} \quad (48)$$

505 The translation coefficient, z_0 , can be interpreted as the zero-plane displace-
 506 ment height. Here, for the sake of our own self-consistency, the notations, d
 507 and z_0 , are other way round from those commonly-adopted in the atmospheric
 508 boundary-layer literature. We now choose the constant $-u_0/a_z = u_*/\kappa$, and
 509 assume stationarity so that C_u , C_1 and C_2 do not depend on X_t . We further
 510 set $C_u = \mathcal{C}u_*$ with \mathcal{C} a constant.

511 Under these assumptions, the logarithmic profile reduces to:

$$\bar{u} = \frac{u_*}{\kappa} \ln \left[\frac{(z-z_0)}{d} \right] + \mathcal{C}u_*. \quad (49)$$

512 Change of the surface roughness, d , produces a shift of the mean velocity,
 513 although the velocity gradient does not explicitly depend on d . The fluxes,
 514 \overline{uw} and $\overline{w^2}$, do not depend on d , either, by assuming both C_1 and C_2 are
 515 constants. These conclusions are compatible with a standard assumption of
 516 constant (in time and space) fluxes in the surface layer, *i.e.*, $\overline{uw} = \overline{uw}_0 = -u_*^2$
 517 and $\overline{w^2} = \overline{w^2}_0$.

518 We use the analogous arguments to solve a hyperbolic system for the buoy-
 519 ancy, taking into account of the additional symmetry (26f), that holds under

the neutral stratifications. Thus,

$$\overline{wb} = \overline{wb_0}, \quad (50)$$

$$\bar{b} = \frac{b_*}{\kappa} \ln \left[\frac{(z - z_0)}{d} \right] + \mathcal{C}' b_* \quad (51)$$

with $a_b = 0$, $a_s = 0$ and $a_t = a_z$, where \mathcal{C}' is another constant.

Alternatively, we can consider the case with non-zero translational constants $uw_0 \neq 0$ and $w_0^2 \neq 0$ in the system Eq. (47). These choices lead to logarithmic solutions for the fluxes, as observed by e.g., for the variance and higher-order statistics of longitudinal velocity (Katul et al., 2016) and for \overline{uw} in case of strong accelerations (Araya et al., 2015).

7.2 Stratified flows

The presence of non-zero buoyancy in the momentum equations leads to a two-way coupling between the velocity and the buoyancy. As a result, the transformation (26f) is further constrained by an additional condition $a_b = a_z - 2a_t$, as discussed in Yano and Waclawczyk (2023), and transformations of \bar{b} are described by Eqs. (26d)–(26e). The fluxes will be constant in time and with height under the condition $a_t = a_z = a_s = 0$, which implies $\beta = \chi = 0$ from Eq. (31h). Thus, the mean wind and buoyancy follow the linear profiles. With $\beta = 0$ and $\chi < 0$, the similarity functions increases more slowly with height. This was observed by Grachev et al. (2013), who found $\phi_m \sim \xi^{0.3}$. After removing data with $Ri > 0.2$ and $R_f > 0.2$, Grachev et al. (2013) concluded that the remaining results follow the MOST predictions very closely. This indicates a local collapse of turbulence at a very large stratification, leading to a significant departure from the MOST prediction.

General invariant solutions in the surface layer can be derived from the invariants (31a)–(31g) in the following manner. Unlike the outer-layer scaling in Section 6, the shift, z_0 , is no longer related to any external length scale, and it can be assumed small. To arrive at the similarity solutions with the local Obukhov length, Λ , as before, we rearrange these coefficients as follows:

$$S = \tilde{C}_u (z - z_0)^{\chi - \beta}, \quad N^2 = \tilde{C}_b (z - z_0)^{\chi - 2\beta}, \quad (52a)$$

$$C_1 = \overline{uw}' (z - z_0)^{2\beta - 2 - \chi}, \quad (52b)$$

$$\frac{C_1}{C_2} = \frac{\overline{uw}'}{w^{2'}}, \quad (52c)$$

$$\frac{C_3}{C_1} = \frac{\overline{wb}'}{\overline{uw}'} (z - z_0)^\beta, \quad (52d)$$

$$X_t \frac{C_3}{C_1} = (t - t_0) \frac{\overline{wb}'}{\overline{uw}'}, \quad (52e)$$

546 where the prime indices suggest deviations of fluxes from the surface values:

$$\overline{uw}' = \overline{uw} - \overline{uw}_0, \quad (53a)$$

$$\overline{wb}' = \overline{wb} - \overline{wb}_0, \quad (53b)$$

$$\overline{w^2}' = \overline{w^2} - \overline{w^2}_0. \quad (53c)$$

547 The invariant relations (52a)–(52e) can be deduced in analogous manner as in
 548 the outer layer, as presented in Sec. 6.2, with a major difference of the mean
 549 profiles being represented in terms of the flux perturbations defined by Eqs.
 550 (53a)–(53c). The results are rather unintuitive, and full implications are still
 551 to be fully investigated.

552 Alternatively, Eqs. (52b)–(52e) can be presented in terms of the vertical
 553 derivatives of fluxes or their gradients, assuming that the time dependence is
 554 weak. Thus,

$$\frac{C_1}{C_2} = \frac{d\overline{uw}}{d\overline{w^2}}, \quad (54a)$$

$$\frac{C_3}{C_1} = \frac{d\overline{wb}}{d\overline{uw}}(z - z_0)^\beta, \quad (54b)$$

$$X_t \frac{C_3}{C_1} = (t - t_0) \frac{d\overline{wb}}{d\overline{uw}}. \quad (54c)$$

555 Even though relations (54a)–(54c) contain gradients rather than the fluxes,
 556 under certain conditions there may exist a relationship between the gradients
 557 and the Obukhov length, Λ . To see this, first recall the definition of the local
 558 Obukhov length, Λ , given by (4), and assume that this length remains approx-
 559 imately constant in the surface layer $\Lambda \approx L$ so that its differential is close to
 560 zero:

$$-d\Lambda = d \left[\frac{|\overline{uw}|^{3/2}}{\overline{wb}} \right] = \frac{3}{2} \frac{(\overline{uw})^{1/2}}{\overline{wb}} d|\overline{uw}| - \frac{(\overline{uw})^{3/2}}{\overline{wb}^2} d\overline{wb} \approx 0. \quad (55)$$

561 It follows from the above expression that under the assumption $\Lambda \approx L$,

$$\left(\frac{d\overline{wb}}{d\overline{uw}} \right) \approx -\frac{3}{2} \frac{\overline{wb}}{\overline{uw}} = -\frac{3}{2} \frac{\sqrt{|\overline{uw}|}}{\kappa\Lambda}, \quad (56)$$

$$\left(\frac{d\overline{wb}}{d\overline{uw}} \right)^2 \approx \frac{9}{4} \frac{\overline{wb}^2}{\overline{uw}^2} = -\frac{9}{4} \frac{\overline{wb}}{\sqrt{|\overline{uw}|}} \frac{1}{\kappa\Lambda}. \quad (57)$$

562 Similar arguments apply for the ratio $d\overline{uw}/d\overline{w^2}$. Under the assumption $\overline{uw} \approx$
 563 $\overline{w^2}$ we obtain

$$\frac{d\overline{uw}}{d\overline{w^2}} \approx \frac{\overline{uw}}{\overline{w^2}}. \quad (58)$$

564 Proceeding similarly as in Section 6.2, we obtain the following functional
565 forms of S and N^2 :

$$S = - \left(\frac{d\overline{wb}}{d\overline{uw}} \right) \left(\frac{z - z_0}{L} \right)^x F \left(\frac{d\overline{uw}}{d\overline{w^2}} \right), \quad (59a)$$

$$N^2 = \left(\frac{d\overline{wb}}{d\overline{uw}} \right)^2 \left(\frac{z - z_0}{L} \right)^x H \left(\frac{d\overline{uw}}{d\overline{w^2}} \right), \quad (59b)$$

566 where we introduced the Obukhov length $L = -|\overline{uw_0}|^{3/2}/(\kappa\overline{wb_0})$ for dimen-
567 sional consistency. The definition $Ri = N^2/S^2$ now implies

$$Ri = \frac{H}{F^2} \left(\frac{z - z_0}{L} \right)^x. \quad (60)$$

568 Solving Eq. (60) for $(z - z_0)/L$, and substituting back to Eqs. (59a) and (59b),
569 we obtain

$$S = - \left(\frac{d\overline{wb}}{d\overline{uw}} \right) \frac{1}{Ri} G \left(\frac{d\overline{uw}}{d\overline{w^2}} \right), \quad (61a)$$

$$N^2 = \left(\frac{d\overline{wb}}{d\overline{uw}} \right)^2 \frac{1}{Ri} G^2 \left(\frac{d\overline{uw}}{d\overline{w^2}} \right), \quad (61b)$$

570 where $G = H/F$. Eqs. (61a) and (61b) do not depend explicitly on χ .

571 Functions (61a) and (61b) reduce to the Monin and Obukhov (1954) scaling
572 predictions at large stratification limit, if Eqs. (56) and (57) hold and $F =$
573 $const$, $H = const$, $Ri = 0.2$. In this case, by setting $G = 2/3$, we obtain

$$S \approx 5 \frac{\sqrt{|\overline{uw}|}}{\kappa\Lambda} \approx 5 \frac{u_*}{\kappa L}, \quad N^2 \approx -5 \frac{\overline{wb}}{\sqrt{|\overline{uw}|} \kappa\Lambda} \frac{1}{\kappa L} \approx 5 \frac{b_*}{\kappa L}. \quad (62)$$

574 Equations (61a) and (61b) are more general than (62), because they take
575 into account of possible variations of the fluxes and dependence on $d\overline{uw}/d\overline{w^2}$.
576 However, for $G > 0$, S is positive only if $d\overline{wb}/d\overline{uw} < 0$. Recall the sign
577 convention for S (*cf.*, Eq. 56). The condition $\Lambda \simeq L$ breaks down, when the
578 gradient $d\overline{wb}/d\overline{uw}$ changes its sign: this happens with strong stratifications, as
579 reported by Grachev et al. (2005). In this case, either of the solutions presented
580 in Section 6, for the outer layer scaling should be used, or alternatively, we can
581 consider that \overline{wb} is increasing from its minimum value and change the sign in
582 the formula (59a).

583 In the surface layer, where Eqs. (56) and (58), are satisfied, formulas (61a)
584 and (61b) can be rewritten in terms of ϕ_m and ϕ_h as:

$$\phi_m \propto \frac{\xi}{Ri} G \left(\frac{\overline{uw}}{w^2} \right), \quad (63a)$$

$$\phi_h \propto \frac{\xi}{Ri} G^2 \left(\frac{\overline{uw}}{w^2} \right). \quad (63b)$$

585 The resulting turbulent Prandtl number in the surface layer is not constant,
 586 but is expressed as a function of the aspect ratio, \overline{uw}/w^2 :

$$Pr_t = \frac{\phi_h}{\phi_m} = G\left(\frac{\overline{uw}}{w^2}\right). \quad (63c)$$

587 8 Data analysis

588 8.1 Estimation of scaling exponents

589 The first goal of the data analysis is to evaluate the scaling exponents, β and
 590 χ , in Eqs. (31b) and (31c). The theory does not predict their values. However,
 591 non-zero χ has implications for the scaling laws derived in Sections 6 and
 592 7. Note that the exponents, β and χ , should remain the same regardless of
 593 whether surface or local scaling is used.

594 In the analysis, we adopt a hypothetical log-linear profile as a reference,
 595 and compare it with the experimental data from SHEBA campaign (Persson et
 596 al., 2002). We expect that β and χ estimated from the SHEBA data will differ
 597 from the corresponding reference estimates, especially at large stratifications.
 598 Particularly, the estimated χ would be non-zero with strong stratifications,
 599 due to the presence of intermittency, in SHEBA data. The standard local
 600 similarity theory assumes $\chi = 0$.

601 The SHEBA campaign, from which data are taken from, took place from
 602 Oct 1997 to Oct 1998 on board of a Canadian icebreaker frozen into the Arctic
 603 ice pack. Turbulent fluxes and mean meteorological data were collected at five
 604 levels on a 20m tower. Turbulent covariances available in the database are
 605 calculated with the 1-h averaging window. The measurement carried out on
 606 the Arctic offers several advantages in SBL studies over those on the mid-
 607 latitudes. During the polar night, a long-lasting SBL can be quasi stationary.
 608 Moreover, a surface covered with snow and ice is usually flat, uniform, and
 609 with no large-scale slope. Thus, data is not contaminated by katabatic flows.
 610 The data are post-processed as outlined in Grachev et al. (2005): especially,
 611 the low-frequency components of covariances are removed to filter-out the
 612 effect of gravity waves.

613 According to MOST, the states with non-zero stratifications are described
 614 by a sum of the linear and logarithmic profiles:

$$\frac{\bar{u}}{u_*} = \frac{1}{\kappa} \ln\left(\frac{z}{d}\right) + 5\frac{z}{L}, \quad \frac{\bar{b}}{b_*} = \frac{Pr}{\kappa} \ln\left(\frac{z}{d}\right) + 5\frac{z}{L}. \quad (64)$$

615 In contrast, this work predicts that the mean wind and buoyancy depend on
 616 height by power laws (*cf.*, Eqs. 31b and 31c). They may approximate Eqs.
 617 (64) locally. Particularly, with the coefficient $\beta = 0$, the power-law solutions
 618 approach linear function as $\chi \rightarrow 0$. On the other hand, as $\chi \rightarrow -1$, the
 619 solutions approach logarithmic, as in this case $S \propto z^{-1}$ and $N^2 \propto z^{-1}$. If
 620 experimental data do not follow the log-linear profile, χ will not reach zero

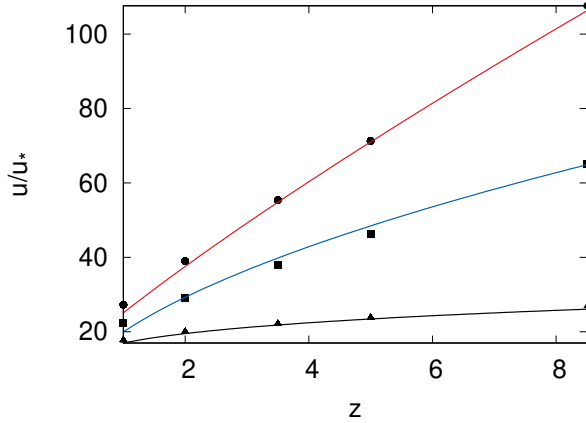


Fig. 1 Log-linear wind speeds (64) marked as symbols: $L = 0.5$ m (circles), $L = 1$ m (squares) and $L = 10$ m (triangles) and respective profiles fitted according to formula (65a) marked as curves.

621 at large stratifications. We verify these expectations first by referring to the
 622 numerically-generated MOST solution (64) and next using experimental data
 623 of SBL.

624 By focusing on the surface layer, we assume that $u_0 = b_0 = 0$ in Eqs. (31b)
 625 and (31c). In this case, Eqs. (31b) and (31c) reduce to:

$$\bar{u} = C_1(z - z_0)^{1-\beta+\chi} = C_u(z - z_0)^{A_u}, \quad (65a)$$

$$\bar{b} = C_2(z - z_0)^{1-2\beta+\chi} = C_b(z - z_0)^{A_b}. \quad (65b)$$

626 The forms (65a), (65b) are fitted to the solution (64) locally, i.e. in the vicinity
 627 of certain height $z = z_1$, such that optimal values of β and χ are chosen.
 628 When fitting the power-law solutions (31b) and (31c) to the reference, log-
 629 linear profile, the exponents $A_u = 1 - \beta + \chi$ and $A_b = 1 - 2\beta + \chi$ in Eqs. (65a)
 630 (65b) should change from values close to zero in the neutral state to unity in
 631 the stratified case (typically for $\xi > 1$). This is illustrated in Fig. 1, in which
 632 log-linear wind speeds (64) with $d = 10^{-4}$ m and $L = 0.5$ m, 1 m and 10 m
 633 are presented by varying symbols at five vertical levels, z . The curves fitted
 634 to Eq. (65a) are also plotted: the estimated exponents A_u are equal to 0.89,
 635 0.73 and 0.28 for $L = 0.5$ m, 1 m and 10 m, respectively.

636 The same procedure can be used to analyze buoyancy profiles, and estimate
 637 the exponent A_b from Eq. (65b). Having the two exponents A_u and A_b , we
 638 can next calculate values for β and χ from the two-equation system:

$$\beta = A_u - A_b, \quad (66)$$

$$\chi = 2A_u - A_b - 1. \quad (67)$$

639 Since our interest here is to estimate the exponents, β and χ , and not the
 640 coefficients C_u and C_b in Eqs. (65a), (65b), we consider the ratios of respective

641 quantities at two different heights. We also take $z_0 \approx 0$ to simplify the analysis,
 642 because our preliminary test concluded that a finite z_0 does not influence the
 643 estimates of scaling coefficients considerably. Thus, we set:

$$\frac{\bar{u}(z_i)}{\bar{u}(z_j)} = \left(\frac{z_i}{z_j}\right)^{A_u}, \quad \frac{\bar{b}(z_i)}{\bar{b}(z_j)} = \left(\frac{z_i}{z_j}\right)^{A_b}. \quad (68)$$

644 As a reference to compare with the observational data, we first generate the
 645 values of \bar{u} and \bar{b} at 5 levels, using the hypothetical “perfect” log-linear profiles
 646 as given in Eqs. (64), *i.e.*, MOST data. The adopted heights are comparable
 647 to those of SHEBA instruments. We assume $d = 10^{-3}$ m and test values of
 648 L in the range $[0.1, 100]$. The data was divided into 20 logarithmically spaced
 649 bins based on the value of the similarity parameter at the first level $\xi_1 =$
 650 z_1/L . In every bin, all possible ratios of values at different vertical levels are
 651 calculated according to the formulas (68). The function $f(z) = az^p$ was fitted
 652 to these data using the nonlinear least squares algorithm in MATLAB Fitting
 653 Toolbox. We mark the fitting error based on a 95% confidence parameter in
 654 the following.

655 The obtained A_u and A_b values for MOST data are presented in Fig. 2 by
 656 circles. As expected, both coefficients are small with weak stratifications, where
 657 the solution is close to logarithmic and increase with the increasing stratifica-
 658 tions towards unity as the MOST solution (64) asymptotically approaches to
 659 the linear profile.

660 The corresponding coefficients β and χ calculated from Eqs. (66) and (67)
 661 for MOST data are presented in Fig. 3 by circles: β remains close to zero for
 662 a full range of ξ ; χ is always negative, and approaches -1 with the decreasing
 663 stratifications. As argued by Yano and Waclawczyk (2023), these solutions
 664 allow both \bar{u} and \bar{b} to be logarithmic in stratified flows. Here, non-zero χ does
 665 not represent the intermittency understood as alternating laminar-turbulent
 666 regimes, but merely reflects a fact that the solution (64) is a sum of two
 667 different contributions: logarithmic and linear. As the stratification increases,
 668 χ approaches 0.

669 In real atmospheric boundary layer flows, the solutions deviate from the
 670 MOST predictions with strong stratifications, where turbulence locally col-
 671 lapses (Klipp and Mahrt, 2004). As a result, the coefficient χ should be smaller
 672 than the one calculated from the MOST profile Eq. (64). To investigate this
 673 possibility, we have performed an equivalent analysis for data from the SHEBA
 674 experiment. We have calculated the buoyancy based on the definition (2). Here,
 675 θ is the 1-hour averaged air temperature measured at the instrument heights
 676 z_n ($n = 1-5$); θ_0 is taken as the 1-hour averaged surface temperature; θ_m is the
 677 average over the five instrument measurements.

678 As before, the data was divided into 20 logarithmically spaced bins based
 679 on the non-dimensionalized value of the first measurement level, $\xi_1 = z_1/L$.
 680 We used the same MATLAB Fitting Toolbox to fit the data according to Eqs.
 681 (68). Resulting A_u and A_b exponents for varying ξ_1 are shown in Fig. 2 by
 682 squares. With weak stratifications, $A_u \approx 0.1$, and with increasing ξ_1 , A_u in-
 683 creases to approximately 0.4. It does not reach the value of 1 predicted by

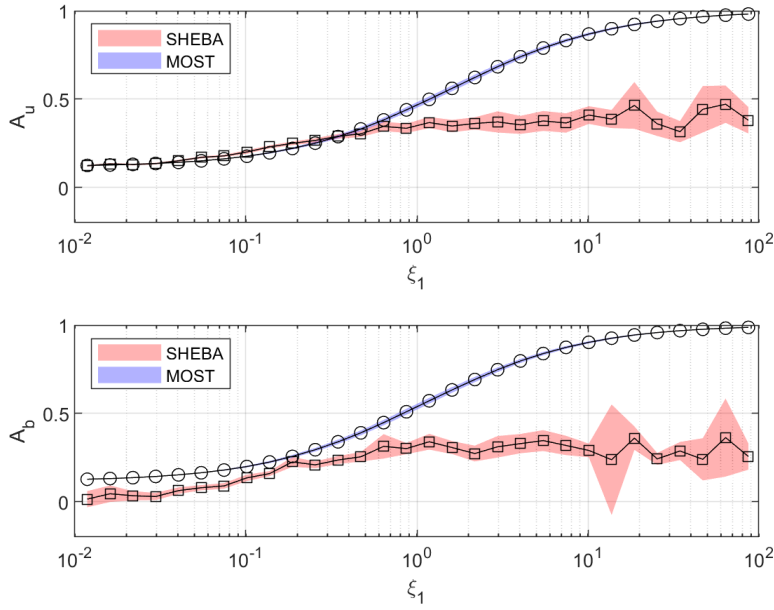


Fig. 2 Exponents a) A_u b) A_b defined in Eqs. (65a) and (65b) calculated for the theoretical profile (64) (circles) and from SHEBA data (squares) together with 95% confidence intervals.

684 the MOST. With very weak stratifications, $\xi_1 \sim 10^{-2}$, the estimated A_b expo-
 685 nent becomes close to zero. In this case, calculating a gradient of temperature
 686 becomes difficult, as the temperature varies only weakly with height. As ξ_1 in-
 687 creases, A_b also increases towards 0.3–0.4. Here again, deviation of the profile
 688 from the MOST solution (64) is visible: both A_u and A_b start to deviate from
 689 the theoretical predictions at ξ_1 in the range between 10^{-1} and 10^0 . According
 690 to Grachev et al. (2005), it is the range where the buoyancy flux $\overline{w\bar{b}}$ start to
 691 increase with height.

692 Corresponding β and χ values are plotted in Fig. 3: β remains close to
 693 zero for a full range of ξ_1 , whereas $\chi \approx -0.8$ towards the weak stratifications,
 694 and it tends to increase with increasing ξ_1 , although it is not easy to draw a
 695 definite conclusion from Fig. 3 due to the large uncertainty in the estimates.
 696 Nevertheless, it is evident that for $\xi_1 > 1$, χ estimated from the SHEBA data is
 697 significantly smaller than MOST data assuming the profile (64). We interpret
 698 it as a result of global intermittency, in which turbulence has a tendency to
 699 form layers with smaller gradients of mean wind and buoyancy than predicted
 700 by MOST.

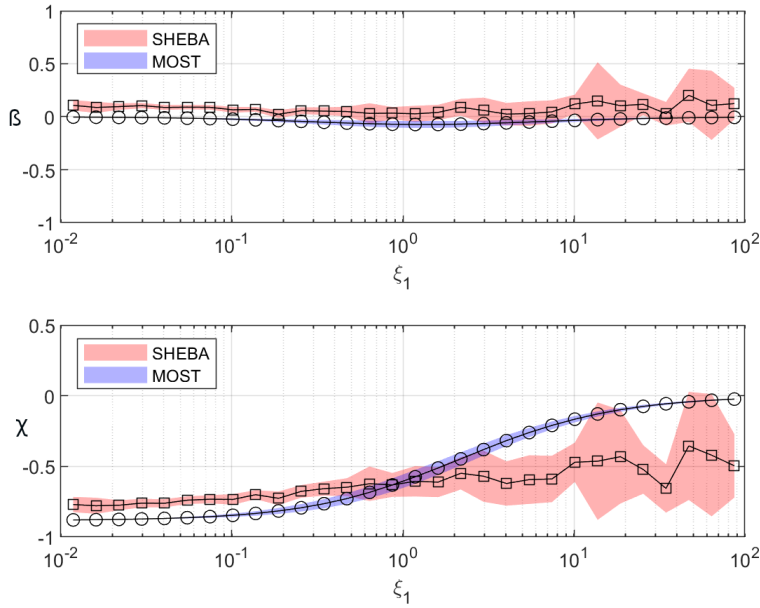


Fig. 3 Same as in Fig. 2 but for exponents β and χ calculated from Eqs. (66) and (67).

701 8.2 Estimation of ϕ_m and ϕ_h and Pr_t

702 Next, we verify the prediction (63c) on the turbulent Prandtl number. Ac-
 703 cording to Eq. (63c), this non-dimensional parameter is not constant, not as
 704 predicted by MOST, but it is a function of \overline{uw}/w^2 or time. Unfortunately, the
 705 time dependence, $(t-t_0)\overline{wb}/\overline{uw}$, is difficult to investigate with only one-hourly
 706 data available. The Pr_t -dependence on the ratio, \overline{uw}/w^2 , is plotted in Fig. 4: it
 707 increases with the increasing \overline{uw}/w^2 . To investigate how the argument changes
 708 with stratification, we also color-code the logarithm of non-dimensional height,
 709 $\ln(\xi)$, in this figure, where $\xi = z/L$. Small \overline{uw}/w^2 tends to correspond to large
 710 ξ . As ξ decreases, the parameter \overline{uw}/w^2 increases towards the value 0.9 at
 711 neutral conditions; Pr_t decreases with increasing stratifications, which was
 712 also confirmed in an earlier study by Sorbjan and Grachev (2010). Those au-
 713 thors plotted Pr_t calculated from SHEBA data as a function of Ri . Larger
 714 scatters of Pr_t with weaker stratifications stem from the increasing difficulties
 715 in estimating gradients of temperature and temperature fluxes in this limit.

716 We further verify the formulas (63a, b) rewritten here for clarity:

$$\phi_m = \frac{\xi}{Ri} G\left(\frac{\overline{uw}}{w^2}\right), \quad \phi_h = \frac{\xi}{Ri} G^2\left(\frac{\overline{uw}}{w^2}\right). \quad (69)$$

717 Assumptions needed to arrive at (69) are that $\Lambda \approx const$ and $d\overline{uw}/d\overline{w^2} \approx$
 718 $const$, so that $d\overline{uw}/d\overline{w^2} \approx \overline{uw}/\overline{w^2}$. Formulas (69) should remain true also

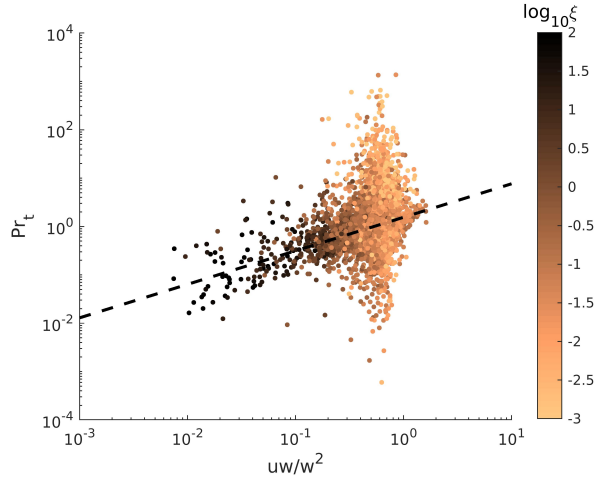


Fig. 4 Pr_t as a function of \overline{uw}/w^2 . Color coded is the logarithm $\log_{10}(\xi)$.

719 with non-zero parameter χ . The dependence of Pr_t on \overline{uw}/w^2 , as defined
 720 as a function, G , by Eq. (63c), was roughly estimated from Fig. 4 as $G \approx$
 721 $1.1(\overline{uw}/w^2)^{0.7}$

722 In Figs. 5 and 6, we plot ϕ_m and ϕ_h against the right-hand sides of Eqs.
 723 (69). All terms are calculated from the SHEBA data for all measurement levels.
 724 The predictions of Eq. (69) are plotted as solid lines. Data points corresponding
 725 to larger stratifications follow the predictions more closely than those of smaller
 726 ξ . However, some of the points clearly follow a different power laws, marked
 727 by dashed lines on both plots, which are defined by:

$$\phi_m \propto \left(\frac{\xi}{Ri} G \right)^{1/3}, \quad \phi_h \propto \left(\frac{\xi}{Ri} G^2 \right)^{-1}. \quad (70)$$

728 These power laws actually correspond to logarithmic solutions for $G \approx const$,
 729 which can be verified after substituting definitions of ϕ_m , ϕ_h , $\xi = z/L$ and Ri
 730 into (70):

$$N^2 \equiv \frac{d\bar{b}}{dz} \sim \frac{b_*}{\kappa z}, \quad S \equiv \frac{d\bar{u}}{dz} \sim \frac{u_*}{\kappa z}. \quad (71)$$

731 The formula (70) is consistent with (69) when $z/L \sim Ri$. The former condition
 732 is not fulfilled exactly with weak stratifications due to large relative errors of
 733 $\bar{w}b$ and N^2 , resulting in large estimation uncertainties of Ri and L . In this
 734 regime, the solutions still follow the scaling (70), which is satisfied by the
 735 logarithmic function, in spite of the errors in estimating L and Ri . Also note
 736 that the relations (70) do not result directly from the Lie group analysis, but
 737 they are rather considered a generalization of Eq. (69). Other possible reasons
 738 for the deviations in Figs. 5 and 6 is that the assumption of $A \approx const$ may no
 739 longer be satisfied with very strong stratifications, where a scatter of data is
 740 also considerable. Variability of $d\overline{uw}/d\overline{w^2}$ may also contribute to the observed
 741 deviations.

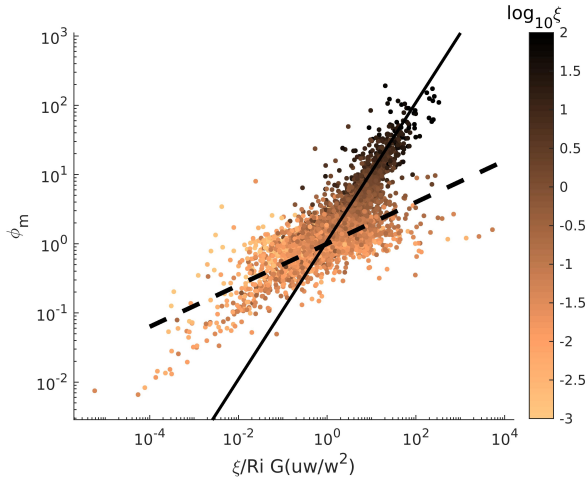


Fig. 5 ϕ_m as a function of ξ/RiG . SHEBA data: symbols, predictions (69): solid line, predictions (70): dashed line. Color coded is the logarithm $\log_{10}(\xi)$.

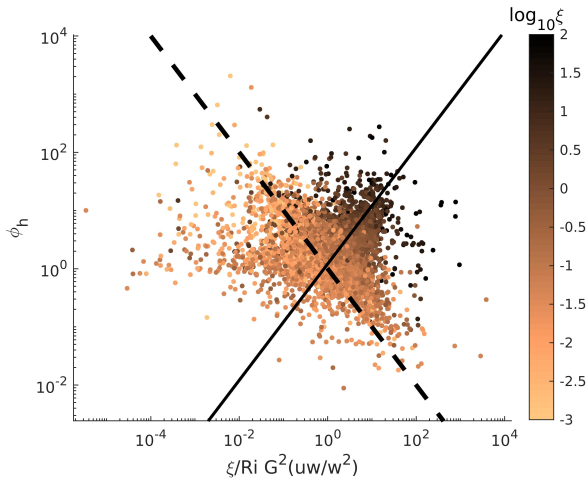


Fig. 6 ϕ_h as a function of ξ/RiG^2 . SHEBA data: symbols, predictions (69): solid line, predictions (70): dashed line. Color coded is the logarithm $\log_{10}(\xi)$.

742 9 Conclusions

743 In this work, we have shown that the local similarity theories of ABL can be
 744 derived by analysis of a governing set of equations in invariant Lie-group
 745 forms, for example, given by Eq. (23) for the heat equation (14). Our investi-
 746 gation also takes into account of a possible presence of intermittency due to a
 747 local collapse of turbulence (Ansorge and Mellado, 2014).

748 We have examined the two different regimes of ABL by adopting the two
 749 different approaches. First, we have assumed that the buoyancy and momen-

750 tum fluxes follow the outer-layer scaling, and increase with height from nega-
 751 tive values close to the surface towards zero at $z = h$. The characteristic length
 752 scale, h , has been taken as the ABL height. The derived solutions, (40a, b), for
 753 the non-dimensional similarity functions, ϕ_m and ϕ_h , are not universal, since
 754 they contain the intermittency parameter χ , which cannot be determined *a*
 755 *priori*, and is constant only locally. On the other hand, the turbulent Prandtl
 756 number, Pr_t , in the invariant form, Eq. (41), obtained from the ratios between
 757 the two similarity functions, ϕ_m and ϕ_h , does not depend on χ . Yet, the form
 758 also predicts that the turbulent Prandtl number, Pr_t , is not constant, either,
 759 but depend on the ratio of the Reynolds stresses, \overline{uw}/w^2 , or alternatively,
 760 the non-dimensional time, $(t - t_0) \overline{wb}/\overline{uw}$. Identifying these two invariants as
 761 arguments of the similarity functions is remarkable, especially considering an
 762 adopted truncation of the system into the mean momentum and buoyancy
 763 prognostic equations. The ratio, \overline{uw}/w^2 , may be considered a measure of flow
 764 anisotropy, or alternatively to be an aspect ratio of eddies. Furthermore, the
 765 same dependency can be re-interpreted in terms of a transiency of the sys-
 766 tem. This further suggests an intimate link between the transiency and the
 767 anisotropy of the flows. We have also demonstrated that our solutions reduce
 768 to the gradient-based similarity theory by Sorbjan (2006) by setting $\chi = 0$.

769 In the second approach, we have considered the surface-layer scaling, in
 770 which the fluxes vary only little with height. Typically, close to the surface,
 771 \overline{uw} will increase with height, and \overline{wb} will decrease with increasing $\xi = z/L$.
 772 No external length scale is introduced in this case. We obtain relations for S
 773 and N^2 as functions of gradients of fluxes, as in Eqs. (61a) and (61b): they are
 774 key results from Section 7. When dependence on $d\overline{uw}/dw^2$ and a contribution
 775 of the intermittency is neglected, derived functions reduce to the common
 776 scaling $\phi_m \propto \xi$ and $\phi_h \propto \xi$, predicted by Monin and Obukhov (1954) for large
 777 stratifications.

778 A goal of data analysis in Section 8 has been to estimate values of exponents
 779 β and χ found in the identified invariant solutions, Eqs. (31a)–(31g), for a full
 780 set of both independent and dependent variables of the boundary-layer system
 781 under considerations. We have compared the data from the SHEBA experi-
 782 ment against the theoretical log-linear profiles (64) predicted from MOST. The
 783 coefficient, χ , estimated for the theoretical profiles (64) increases from -1 at
 784 small $\xi = z/L$ to zero towards large ξ , over which the solution is purely linear.
 785 On the other hand, the coefficient χ estimated from SHEBA data levels-off at
 786 around -0.5 . This confirms that both the wind shear and the stratification are
 787 predicted by algebraic scaling laws (34a) and (34b). A difference between the
 788 MOST and experiment increases with the increasing ξ ; it can be attributed to
 789 the presence of global intermittency, which is quantified in our analysis by a
 790 non-zero parameter, χ .

791 In Section 8.2, we have further investigated the validity of the similarity
 792 solutions for ϕ_m , ϕ_h and Pr_t in the surface layer, as derived as Eqs. (63a,
 793 b, c). As predicted, the turbulent Prandtl number, Pr_t , is not constant, but
 794 depends on the measure, \overline{uw}/w^2 , of the anisotropy. Interestingly, data with
 795 stronger stratifications follows the predictions of Eqs. (63a, b) for ϕ_m and ϕ_h

quite closely, whereas for the smaller non-dimensional height, $\xi = z/L$, data rather follows the scalings $\phi_m \propto (\xi/RiG)^{1/3}$ and $\phi_h \propto (\xi/RiG^2)^{-1}$: these forms correspond to logarithmic solutions when $G \approx const$.

There exist various intriguing directions for further studies based on the symmetries of the ABL flows. First, the identified time dependence on solutions (*cf.*, Eq. 36) in this study requires further attentions. Second, the outer-layer scaling investigated in Section 6 and the role of exponent χ should be investigated in more detail based on experimental data and by comparison with existing analyses, *e.g.*, Allouche et al. (2022). Hopefully, derived invariant functions will improve parametrizations of the stable atmospheric boundary layers and provide the basis for turbulence closures which account for the intermittent structure of ABL, such as the stochastic model by Allouche et al. (2021). Finally, the effect of Coriolis force and the resulting modification of symmetries should be accounted for. This may improve predictions at very large stratifications, where the ABL height is relatively small, and the statistics of the whole ABL are influenced by the Earth's rotation.

Data availability. The datasets analysed during this study are available in the repository of the Earth Observing Laboratory:

<https://data.eol.ucar.edu/project/SHEBA>

Post-processed data were made available to us by A. Grachev after our request.

Acknowledgements The financial support of the National Science Centre, Poland (Project No. 2020/37/B/ST10/03695) is gratefully acknowledged. JIY further acknowledges support of IDUB Mentoring Programm of the University of Warsaw.

References

- Allouche M, Bou-Zeid E, Anson C, Katul G G, Chamecki M, Acevedo O, Thanekar S and Fuentes J D (2022) The Detection, Genesis, and Modeling of Turbulence Intermittency in the Stable Atmospheric Surface Layer. *J. Atmos. Sci.* 79:, 1171–1190.
- Allouche M, Katul G G, Fuentes J D, Bou-Zeid E, (2021) Probability law of turbulent kinetic energy in the atmospheric surface layer. *Phys. Rev. Fluids* 6:, 074601.
- Anson C and Mellado JP (2014) Global Intermittency and Collapsing Turbulence in the Stratified Planetary Boundary Layer. *Boundary-Layer Meteorol* 153: 89–116
- Araya G, Castillo L and Hussain F (2015) The log behaviour of the Reynolds shear stress in accelerating turbulent boundary layers. *Journal of Fluid Mechanics* 775: 189–200
- Avsarkisov V, Hoyas S, Oberlack M and García-Galache J (2014) Turbulent plane Couette flow at moderately high Reynolds number. *Journal of Fluid Mechanics* 751: R1.
- Barenblatt GI (1996) *Scaling, Self-Similarity, and Intermediate Asymptotics*, Cambridge University Press, Cambridge, UK.

- 838 Bluman G W, Kumei S (1989) *Symmetries and Differential Equations*,
839 Springer–Verlag, New York.
- 840 Buckingham E (1914) On Physically Similar Systems; Illustrations of the Use
841 of Dimensional Equations, *Phys. Rev.* 4: 345.
- 842 Businger JA, Wyngaard JC, Izumi Y, and Bradley EF (1971) Flux-Profile
843 Relationships in the Atmospheric Surface Layer, *jas* 28:, 181–189.
- 844 Foken T (2006) 50 years of the Monin-Obukhov similarity theory. *Boundary-*
845 *Layer Meteorol* 119: 431–447
- 846 Frewer M, Khujadze G and Foysi H (2015) Comment on “Statistical sym-
847 metries of the Lundgren-Monin-Novikov hierarchy” *Phys. Rev. E* 92:
848 067001
- 849 Grachev A A, Fairall C W, Persson P O, Andreas E L, Guest P S (2005)
850 Stable boundary layer scaling regimes: The SHEBA data, *Boundary-*
851 *Layer Meteorol* 116: 201–235
- 852 Grachev AA, Andreas EL, Fairall CW et al. (2013) The Critical Richardson
853 Number and Limits of Applicability of Local Similarity Theory in the
854 Stable Boundary Layer. *Boundary Layer Meteorol* 147:, 51–82.
- 855 Grachev A A, Andreas E L, Fairall C W, Guest P S and Persson P O G
856 (2015), Similarity theory based on the Dougherty–Ozmidov length scale.
857 *Q.J.R. Meteorol. Soc.* 141: 1845–1856.
- 858 Ji Y and She ZS. (2021) Analytic derivation of Monin-Obukhov similarity
859 function for open atmospheric surface layer. *Sci. China Phys. Mech.*
860 *Astron.* 64: 34711.
- 861 Katul G G, Banerjee T, Cava D, Germano M, Porporato A (2016) Generalized
862 logarithmic scaling for high-order moments of the longitudinal velocity
863 component explained by the random sweeping decorrelation hypothesis.
864 *Physics of Fluids* 28: 095104
- 865 Khujadze G and Oberlack M (2004) DNS and scaling laws from new sym-
866 metry groups of ZPG turbulent boundary layer flow *Theoret. Comput.*
867 *Fluid Dyn.* 18: 391–411
- 868 Klipp C L, Mahrt L (2004) Flux–gradient relationship, self-correlation and
869 intermittency in the stable boundary layer *Q.J.R. Meteorol. Soc.* 130:
870 2087–2103
- 871 Lighthill K (1978) *Waves in Fluids*, Cambridge University Press, Cambridge.
- 872 Loboeki L (2013) Analysis of vertical turbulent heat flux limit in stable condi-
873 tions with a local equilibrium, turbulence closure model. *Boundary-Layer*
874 *Meteorol* 148: 541–555.
- 875 Loboeki L, Porretta-Tomaszewska P (2021) Prediction of gradient-based sim-
876 ilarity functions from the Mellor–Yamada model. *Q J R Meteorol Soc*
877 147: 3922–3939.
- 878 Monin AS, Obukhov AM (1954) Basic laws of turbulent mixing in the surface
879 layer of the atmosphere. *Tr. Nauk SSSR Geophys. Inst.* 24: 163–187 (in
880 Russian: translation available *e.g.*, at:
881 https://mcnaughty.com/keith/papers/Monin_and_Obukhov_1954.pdf)
- 882 Nieuwstadt FTM (1984) The turbulent structure of the stable, nocturnal
883 boundary layer. *J. Atmos. Sci.* 41: 2202–2216.

- 884 Oberlack M (2001) A unified approach for symmetries in plane parallel tur-
885 bulent shear flows. *Journal of Fluid Mechanics* 427: 299–328.
- 886 Oberlack M, Rosteck A, (2010) New statistical symmetries of the multi-point
887 equations and its importance for turbulent scaling laws. *Discrete and*
888 *Continuous Dynamical Systems - S* 3:, 451–471.
- 889 Oberlack, M., S. Hoyas, S. V. Kraheberger, F. Alcántara-Ávila, and J. Laux,
890 (2022) Turbulence statistics of arbitrary moments of wall-bounded shear
891 flows: A symmetry approach. *Phys. Rev. Lett.* 128:, 024502.
- 892 Obukhov AM (1948) Turbulence in an atmosphere with a non-uniform tem-
893 perature. *Trans. Inst. Theoretical Geophysics* 1: 95–115 (in Russian:
894 translation in *Boundary-Layer Meteorol* 2:(1971), 7–29)
- 895 Persson P O G, Fairall C W, Andreas E L, Guest P S and Perovich D K
896 (2002) Measurements near the Atmospheric Surface Flux Group Tower
897 at SHEBA: Near-Surface Conditions and Surface Energy Budget, *J. Geo-*
898 *phys. Res.* 107: 8045.
- 899 Pukhnachev V V (1972) Invariant solutions of Navier-Stokes equations de-
900 scribing motions with free boundary, *Dokl. Akad. Nauk* 202: 302.
- 901 Rosteck A (2014) Scaling Laws in Turbulence – A Theoretical Approach
902 Using Lie-Point Symmetries. PhD Thesis, TU Darmstadt, Germany.
- 903 Sadeghi H, Oberlack M and Gauding M (2021). New symmetry-induced scal-
904 ing laws of passive scalar transport in turbulent plane jets. *Journal of*
905 *Fluid Mechanics* 919: A5.
- 906 Sorbjan Z (1989) *Structure of the Atmospheric Boundary Layer*, Prentice
907 Hall, Englewood Cliffs, USA.
- 908 Sorbjan Z (2006) Local structure of stably stratified boundary layer. *J.*
909 *Atmos. Sci.* 63: 1526–1537.
- 910 Sorbjan Z (2010) Gradient-based scales and similarity laws in the stable
911 boundary layer. *Q J R Meteorol Soc* 136: 1243–1254.
- 912 Sorbjan Z, Grachev AA (2010) An Evaluation of the Flux-Gradient Rela-
913 tionship in the Stable Boundary Layer. *Boundary Layer Meteorol* 135:,
914 385–405.
- 915 Sorbjan Z (2012) The Height Correction of Similarity Functions in the Stable
916 Boundary Layer. *Boundary-Layer Meteorol* 142: 21–31.
- 917 Sorbjan Z (2016) Similarity scaling system for stably stratified turbulent
918 flows. *Q J R Meteorol Soc* 142: 805–810.
- 919 Stiperski I and Calaf M (2023) Generalizing Monin-Obukhov Similarity The-
920 ory (1954) for Complex Atmospheric Turbulence. *Phys. Rev. Lett.* 130:,
921 124001
- 922 Stiperski I, Chamecki M and Calaf M., (2021) Anisotropy of Unstably Strat-
923 ified Near-Surface Turbulence. *Boundary-Layer Meteorol* 180:, 363–384
- 924 Waclawczyk M, Staffolani N, Oberlack M, Rosteck A, and Friedrich R (2014)
925 Statistical symmetries of the Lundgren-Monin-Novikov hierarchy. *Phys.*
926 *Rev E* 90:, 023022-1–11.
- 927 Waclawczyk M, Grebenev V N and Oberlack M (2017) Lie symmetry analy-
928 sis of the Lundgren-Monin-Novikov equations for multi-point probability
929 density functions of turbulent flow. *J. Phys. A: Math. Theor.* 50: 175501

- 930 Yano JI, Bonazzola M (2009) Scale analysis for large-scale tropical atmo-
931 spheric dynamics. *J. Atmos. Sci.* 66:, 159–172.
- 932 Yano J and Waclawczyk M (2022) Nondimensionalization of the Atmospheric
933 Boundary-Layer System: Obukhov Length and Monin–Obukhov Similar-
934 ity Theory. *Boundary-Layer Meteorol* 182:, 417–439.
- 935 Yano J and Waclawczyk M (2023) Symmetry Invariant Solutions in Atmo-
936 spheric Boundary Layers submitted to *J. Atmos. Sci.* 81:, 263–277.
- 937 Zilitinkevich S, Calanca P (2000) An extended similarity–theory for the stably
938 stratified atmospheric surface layer. *Q J R Meteorol Soc* 126: 1913–1923.
- 939 Zilitinkevich S and Esau IG (2005) Resistance and heat–transfer for sta-
940 ble and neutral planetary boundary layers: Old theory advanced and re-
941 evaluated. *Q J R Meteorol Soc* 131: 1863–1892.
- 942 Zilitinkevich SS, Esau IN (2007) Similarity theory and calculation of turbu-
943 lent fluxes at the surface for the stably stratified atmospheric boundary
944 layer. *Boundary-Layer Meteorol* 125: 193–205